ELSEVIER

Polymer 43 (2002) 2385–2400

polymer

www.elsevier.com/locate/polymer

Hybrid inorganic–organic materials based on a 6FDA–6FpDA–DABA polyimide and silica: physical characterization studies

Chris J. Cornelius[a,1], Eva Marand[b,*]

[a]*Sandia National Laboratories, P.O. Box 5800, Albuquerque, NM 87185-0710, USA*
[b]*Department of Chemical Engineering, Virginia Polytechnic Institute and State University, Blacksburg, VA 24061-0211, USA*

Received 7 June 2001; received in revised form 29 November 2001; accepted 30 November 2001

Abstract

A series of hybrid polyimide–silica composites were fabricated from a functionalized fluorinated polyimide and tetramethoxysilane (TMOS), methyltrimethoxysilane (MTMOS), and phenyltrimethoxysilane (PTMOS) via a sol–gel process. Polyimides were solution imidized employing 4,4′-hexafluoroisopropylidenediphthalic anhydride (6FDA), and various amounts of 4,4′-hexafluoroisopropylidene dianiline (6FpDA) and 3,5-diaminobenzoic acid (DABA). The degree of cross-linking between the silica structures and the polyimide matrixes, as well as the morphology of the hybrid systems were highly dependent on the type and content of the alkoxide employed. The higher functionality and reactivity of TMOS alkoxide gave rise to highly cross-linked, homogeneous hybrid systems, while the MTMOS and PTMOS based hybrid systems were phase separated and the silica structures largely uncondensed. Although the thermal stability changed a little, incorporation of the silica structures in the polyimide matrix increased the rigidity and mechanical strength of the hybrid materials, particularly at elevated temperatures.

Keywords: Polyimide; Membrane; Gas transport

1. Introduction

In recent years, hybrid materials have found many uses such as abrasive resistant coatings, contact lenses, sensors, optically active films, membranes and absorbents [1–11]. Hybrid inorganic–organic materials can be formed utilizing the sol–gel process via a number of approaches. For example, one method involves the in situ reaction of an alkoxide with an organic polymer or oligomer. Chemical bonding between the alkoxide and oligomer or polymer occurs via functionalized reactive groups, which participate in the alkoxide condensation reactions. These condensation reactions result in the formation of the inorganic network that is covalently bonded to the organic oligomer or polymer [6,12,13]. A similar approach for creating a hybrid inorganic–organic material involves the in situ polymerization of an alkoxide and an organic monomer [14]. Finally, alkoxide precursors can be imbibed into a polymer matrix and then reacted within the swollen polymer to form the final hybrid material [14–19]. All these hybrid systems can exhibit phase separation, which is dependent on the reaction conditions and the degree of compatibility between the organic and inorganic components. The resulting morphology can assume either nano or micro-structural features, which ultimately dictate the final properties of the hybrid material [12–20].

The sol–gel process consists of hydrolysis (Step 1) and condensation reactions (Steps 2 and 3), as shown in Fig. 1 for an arbitrary silicon alkoxide system. These reactions are typically catalyzed with an acid or a base and occur concurrently. The relative rates of the hydrolysis or the condensation reactions are governed by the reaction conditions. The final morphology and properties of the inorganic gel and subsequent glass are dependent on many interdependent variables. Variables such as the alkoxide structure, the pH of the reaction medium, the type of solvent, the ratio of water and catalyst to the alkoxide, the reaction temperature and pressure, and the overall concentration of reactants all contribute to the final morphology and properties [21–25]. In general, if the sol–gel reactions are base catalyzed, the sol morphology will consist of colloidal non-interpenetrating clusters, while the sol morphology of an acid catalyzed alkoxide will tend to be dominated by linear and randomly branched structures [21–25]. Altering the reaction variables will lead to different sol morphologies and final glass or

* Corresponding author. Tel.: +1-540-231-8231; fax: +1-540-231-5022.
E-mail addresses: cjcorne@sandia.gov (C.J. Cornelius), emarand@vt.edu (E. Marand).
[1] Tel.: +1-505-844-6192; fax: +1-505-845-9500.

0032-3861/02/$ - see front matter
PII: S0032-3861(01)00803-5

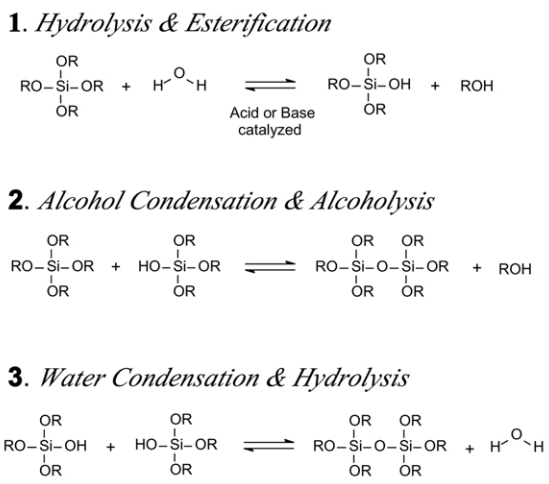

Fig. 1. Sol–gel reactions with silicon alkoxide showing the hydrolysis reaction (1), and the condensation reactions (2 and 3).

xerogel properties. Such studies fall into an extensive field of research known as Sol–Gel chemistry.

The morphology and physical properties of hybrid organic–inorganic materials and the effects of synthetic variables of the sol–gel process have been investigated for a number of polymeric systems [12,13,26]. Controlling the physical properties of the hybrid material is highly dependent on the compatibility of the organic and the inorganic phases, the initial properties of the organic and inorganic constituents, the molecular weight of the organic material, and the size of the organic and inorganic domains. Wilkes et al. prepared ceramic polymers or CERAMERS from silanol terminated oligomers of poly(dimethylsiloxane) and tetraethoxysilane (TEOS) which yielded tough hybrid materials [12]. These studies revealed that increasing the acid content and decreasing the molecular weight of the poly(dimethylsiloxane) oligomer results in highly homogeneous materials with significant decreases in phase separation.

In contrast, attempts at combining high performance polymers, such as polyimides with alkoxysilanes using sol–gel chemistry met with more difficulties. In earlier studies, large, micron-sized inorganic domains were generated with inhomogeneous distribution within the polymer matrix [27,28]. This led to brittle materials with microscopic cracks [27,28]. In order to minimize the size of the ceramic nanoclusters and to prevent their agglomeration, Nandi and co-workers prepared polyimide–SiO_2 and polyimide–TiO_2 hybrids via the 'site isolation method' [29]. This method consisted of pre-binding an alkoxide precursor to a polyamic acid, forming a carboxylate group, and subsequently curing the system to imidize the polyamic acid and to drive the sol–gel reactions. Homogeneously dispersed silica and titania particles, in the order of 1–1.5 nm, were observed in the polyimide matrix, particularly at low oxide loadings, although micron-sized particles were evident at higher oxide loadings (>40%). However, the site-isolation method has had problems with incomplete imidization, since the hydrolysis of the carboxylate groups is slow and the metal precursors remain bound to the polyamic acid until all the alkoxide groups have been hydrolyzed off [29]. Joly et al., who employed the same method to fabricate polyimide–silica membranes, also presented evidence, which suggested that prebinding of the alkoxide precursor prevents complete imidization [11].

Initial attempts by Morikawa et al. to produce polyimide–silica hybrid materials via sol–gel reactions utilizing TEOS and a polyamic acid (PMDA–ODA) resulted in a hybrid material with considerably reduced tensile strength and elongation at break [27]. These results were attributed to poor interfacial bonding between the precipitated silica particles and the polyimide matrix, and gross inorganic phase separation characterized by 3–7 μm diameter particles. Spinu et al. produced very homogeneous polyimide–silica hybrid materials by employing low molecular weight functionalized polyimides [28]. However, these hybrid materials were extremely brittle, possibly as a result of the inadequate polyimide molecular weight necessary for the formation of a tough polyimide film.

Later, Morikawa et al. greatly improved the properties of the PMDA–ODA polyimide hybrids by introducing different types and concentrations of pendant alkoxysilanes along the polyimide backbone [30]. These pendant groups provided connection points to the silica particles, which increased the homogeneity of the polyimide–silica hybrid and produced a much finer dispersion of silica particles. In particular, it was found that trifunctional alkoxysilanes produced more homogeneous hybrid materials than mono- and difunctional pendant alkoxysilanes. The trifunctional alkoxysilane hybrid materials resulted in transparent films containing up to 70% SiO_2. The storage modulus, E', of these hybrid materials increased with increasing silica content with only small decreases in the elongation at break when compared to previous studies [30]. At constant silica content, the glass transition temperature, T_g, of these hybrid materials increased with increasing alkoxysilane pendant concentration. At high alkoxysilane pendant concentration the T_g became indiscernible. This increase in T_g with increasing alkoxysilane pendant concentration is indicative of reduced polyimide chain mobility due to higher degree of covalent bonding between functional side chains and silica domains. The advantage of this approach is the formation of a homogeneous hybrid system, resembling a collection of pseudo-low molecular weight polyimide oligomers tied by silica domains, although the overall high molecular weight of the polyimide is actually high, as required for good mechanical properties.

A study by Kioul and Mascia demonstrated that silane-coupling agents could also be used to improve the compatibility of polyimide–silicate hybrid materials [31]. This approach can be critical when attempting to minimize the degree of phase separation when employing high molecular weight polymers. The use of silane coupling agents yielded hybrid materials, which were highly transparent and had a

very fine dispersion of silica throughout the matrix [26,31]. Unfortunately, thin films created from this hybrid material were still brittle, possibly due to interfacial defects between the silica domains and the polymer matrix.

In this paper we outline a synthesis strategy for hybrid inorganic–organic membrane materials, which overcomes several of the problems discussed earlier, such as brittleness and incomplete imidization. This synthesis strategy allows the sol–gel process to proceed in the presence of a fully imidized high molecular weight polyimide. Because we are primarily interested in developing materials for membrane applications, our focus is on combining highly gas selective and thermally stable polyimides with various alkoxysilanes. Furthermore, we will study the compatibility of organic and inorganic domains by using 3,5-diaminobenzoic acid, DABA, in the polyimide synthesis. The addition of DABA introduces additional functionalities along the polyimide backbone. When reacted with aminopropyltriethoxysilane, APTEOS, coupling agent, the functional groups provide a link between the inorganic domains and the polymer matrix. While the nature of the organic substituent on the organoalkoxysilane can influence the compatibility between the inorganic and organic domains, it also changes the sol–gel kinetics, resulting in different hybrid morphologies and properties. These phenomena are examined in this paper.

2. Experimental

2.1. Materials

Solvents, 1-methyl-2-pyrrolidinone (NMP), and 1,3-dichlorobenzene (DCB) were obtained from Fisher Scientific. The NMP and DCB were dehydrated prior to use by stirring over phosphorous pentoxide (P_2O_5) for 24 h followed by vacuum distillation. The constant boiling fraction was collected and stored in a flame-dried 500 ml round bottom flask and sealed with a ground glass stopper. Because NMP is a hygroscopic solvent, the dehydrated NMP was used for synthesis within one week in order to minimize water absorption. The 37.5 wt% HCl was used as received from Fisher Scientific for the acid catalysis of the various alkoxides. Phenyltrimethoxysilane (PTMOS), methyltrimethoxysilane (MTMOS), and tetramethylorthosilicate (TMOS) were obtained from Aldrich with purity levels of 98, 99 and 99.99%, and used as received. The 4,4′-(hexafluoroisopropylidene) diphthalic anhydride (6FDA) and 4,4′-(hexafluoroisopropylidene) dianiline (6FpDA) were obtained from Clariant Fine Chemicals Division with a purity level of 99%. The 3,5-diaminobenzoic acid (DABA) was obtained from Aldrich and had a purity level of 98%. Prior to using 6FDA, 6FpDA and DABA, these reagents were vacuum dried at 120 °C for five days to remove trace amounts of adsorbed water. The 3-aminopropyltriethoxysilane (APTEOS) was obtained from Aldrich at 99% purity and used as received.

2.2. Polyimide synthesis

A two-step solution-imidization technique was employed to synthesize the 6FDA–6FpDA–DABA (6FDA–6FpDA–DABA-25) polyimide as shown in Figs. 2 and 3. Control of the final molecular weight, and endgroup functionality was achieved by controlling the reactant stoichiometry as predicted by Carothers equation for a step-growth polymer [32]. The synthetic target was an 80 g batch of 75K $\bar{M}_w$ 6FDA–6FpDA–DABA polyimide possessing 2.2K $\bar{M}_w$ 6FDA–6FpDA polyimide segments, dianhydride endgroups, and 25 mol% DABA. This required 107.8 mmol of 6FDA (47.866 g), 53.51 mmol of 6FpDA (17.886 g), and 52.28 mmol of DABA (7.954 g). A stoichiometric excess of 6FDA was used to synthesize the polyimide with dianhydride endgroups.

The first step in the synthesis of the 6FDA–6FpDA–DABA-25 polyimide involved creating a 2.2K $\bar{M}_w$ 6FDA–6FpDA polyimide with dianhydride endgroups. Flame dried 250 ml round bottom flasks were used to create individual solutions from the predicted amounts of 6FDA and 6FpDA. A total of 440 ml of NMP were used to dissolve the reactants and give a 15 wt% polymer solution. The 6FpDA solution was added to a previously flame dried and N_2 purged 1000 ml three-necked round bottom flask, and then followed by the slow addition of the 6FDA solution. An additional 130 ml of DCB was added to the polyamic solution to create a 4:1 molar ratio of NMP and DCB. The polyamic acid was formed after constantly stirring the reactants for 24 h at 25 °C in a N_2 purged atmosphere. The extensive reaction time was used to provide the polyamic acid sufficient time to equilibrate to the desired molecular weight. The polyamic was then thermally imidized for 24 h at 180 °C in a constantly stirred N_2 purged atmosphere. Water formed during cyclodehydration of the polyamic acid formed a low boiling point azeotrope with DCB, which was subsequently distilled and condensed out of the reaction solution. A modified Dean–Stark trap was used to maintain a constant solvent reaction volume by replacing distilled DCB with fresh DCB. After the reaction was complete, the polyimide solution was allowed to cool to room temperature.

The final or second step in the synthesis of the 6FDA–6FpDA–DABA-25 polyimide with dianhydride endgroups was the addition of the predicted amount of DABA to the 2.2K $\bar{M}_w$ 6FDA–6FpDA polyimide solution. As shown in Fig. 3, the polyamic acid solution was constantly stirred in a N_2 atmosphere for 24 h at 25 °C to ensure sufficient time for molecular weight equilibration. After this time interval, the polyamic acid solution was thermally imidized at 180 °C in a constantly stirred N_2 purged atmosphere. Water formed during cyclodehydration of the polyamic acid was removed using the same synthetic method previously described.

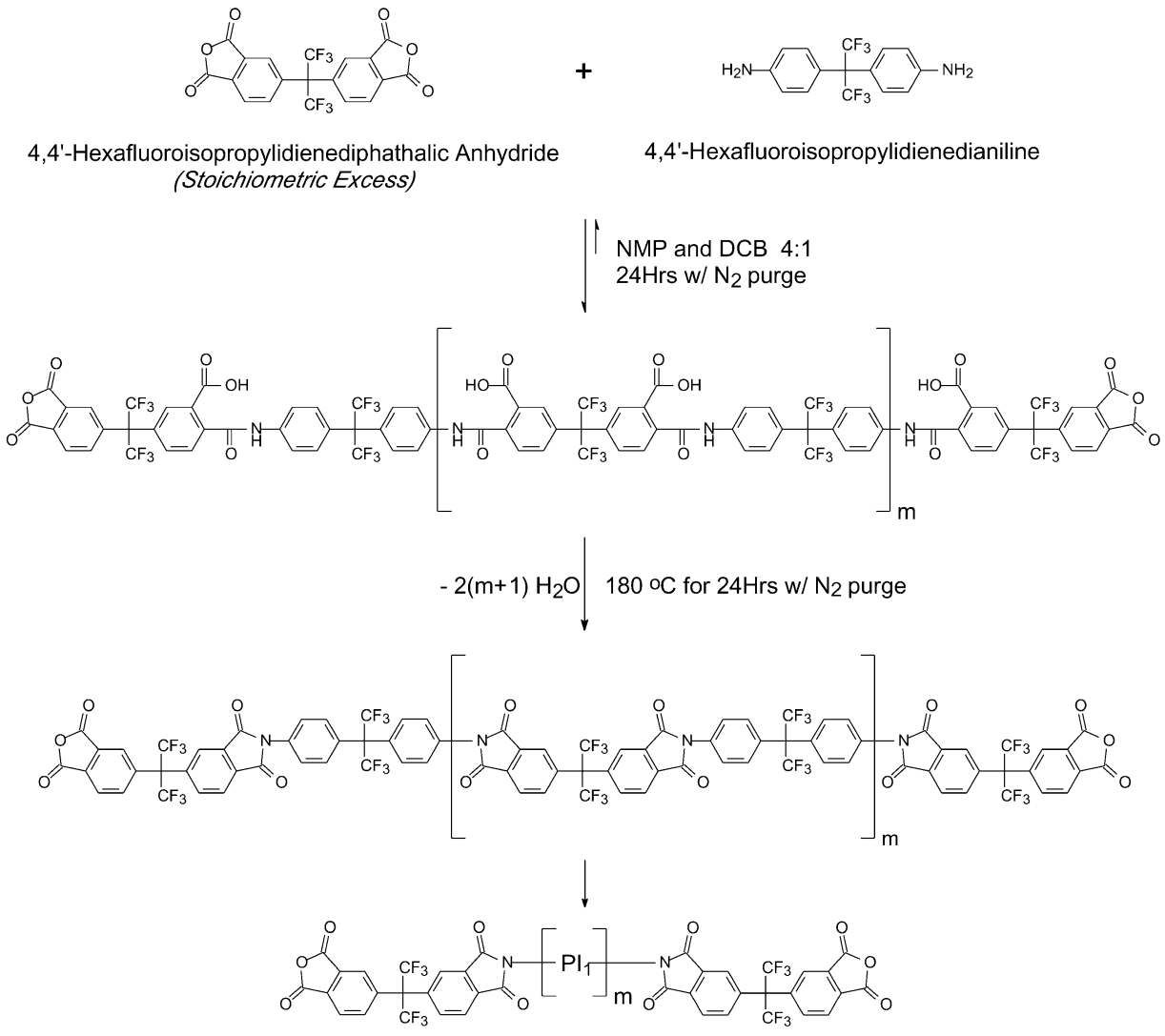

Fig. 2. Synthetic route for polyimide synthesis employing the solution imidization technique.

The final 6FDA–6FpDA–DABA polyimide was cooled to room temperature, filtered with a 5 μm nylon filter, and then precipitated in methanol. A whitish-brown precipitate was recovered and subsequently dried in a vacuum oven at 150 °C for 24 h. After drying the precipitate, it was then dissolved in THF, filtered twice using a 5 μm nylon filter, and then cast in Teflon™ coated pans to form films. These films were then dried for 24 h at 220 °C in a vacuum oven to remove trace amounts of THF, NMP and DCB. As determined by GPC, the final molecular weight and polydispersity (PDI) of this 6FDA–6FpDA–DABA polyimide were 80K $\bar{M}_w$ and 2.4.

2.3. Hybrid synthesis

Hybrid materials were successfully synthesized employing the generalized synthetic approach shown in Figs. 1 and 4. This synthetic technique is based on creating two individual homogeneous inorganic and organic solutions, which are then mixed together and allowed to react at room temperature with carefully controlled evaporation conditions. The first homogeneous inorganic solution is a partially acid hydrolyzed alkoxide sol in THF, while the second homogenous organic solution is an APTEOS functionalized polyimide in THF. An amide is formed between the polyimide acid groups and the amine within the APTEOS via nucleophilic attack, which is also shown in Fig. 4. Furthermore, the presence of the pendant APTEOS groups on the functionalized polyimide facilitates chemical bonding with the partially hydrolyzed alkoxide sol via condensation reactions as shown in Fig. 1. At the completion of the evaporation step of the previously mixed

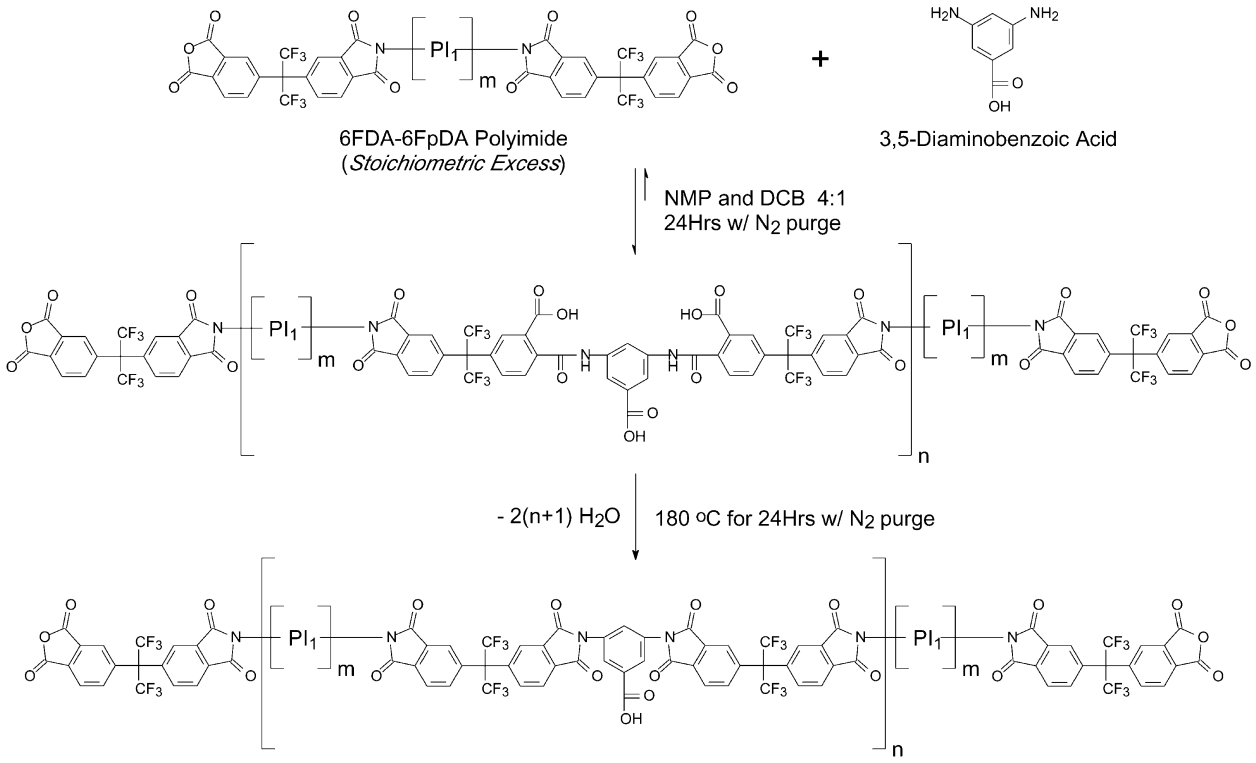

Fig. 3. Synthetic route for polyimide synthesis, incorporating 3,5-diaminobenzoic acid.

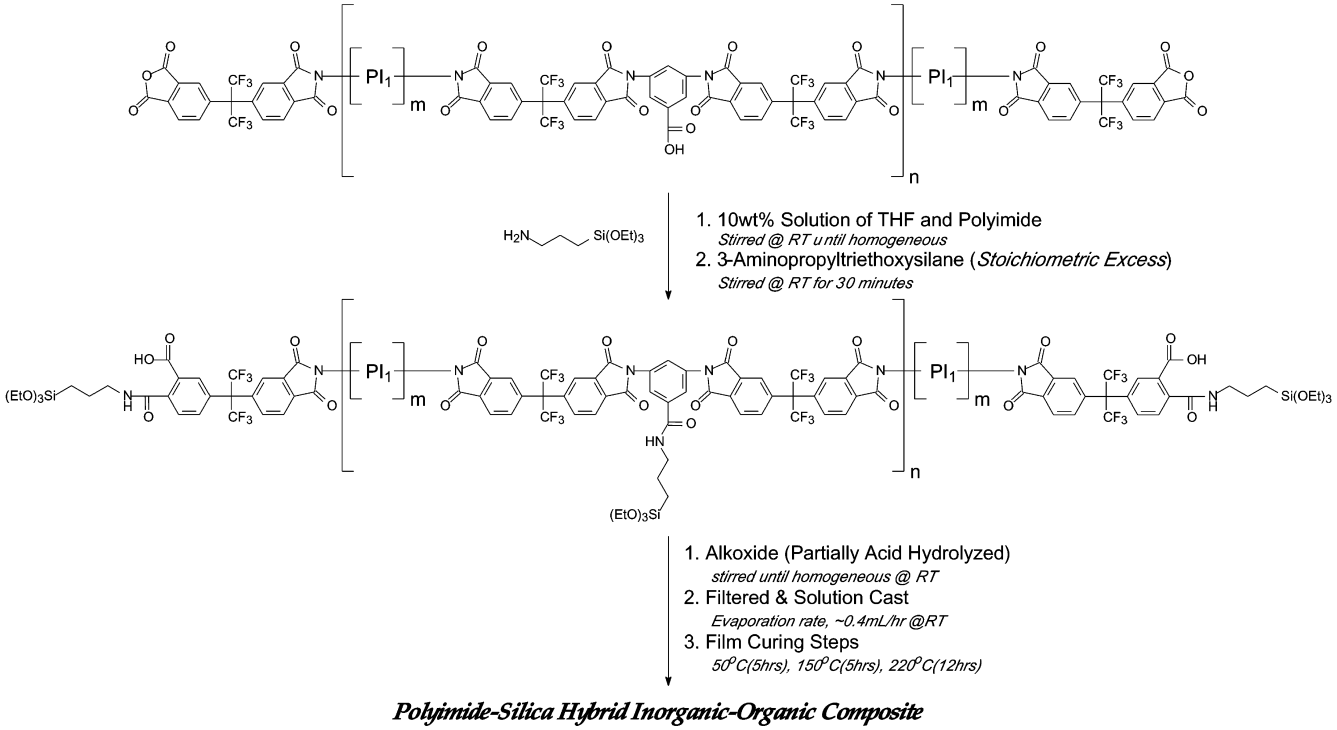

Fig. 4. Synthetic route for polyimide functionalization and conversion to a polyimide–silica hybrid.

Table 1
Reactant summary of 80K $\bar{M}_w$ 6FDA–6FpDA–DABA-25 polyimide and hybrid materials

	Polyimide (g)	Alkoxide (μl)	APTEOS (μl)	HCl[a] (μl)	H_2O (μl)	THF (ml)
6FDA–6FpDA–DABA-25	2.77	0	0	0	0	28.1
7.5 wt% TMOS	2.76	216	187	11.9	43.96	27.9
15 wt% TMOS	2.75	470	187	25.8	95.5	27.8
22.5 wt% TMOS	2.76	774	187	42.5	157	27.8
7.5 wt% MTMOS	2.75	234	187	9.14	33.8	27.9
15 wt% MTMOS	2.75	509	187	19.9	73.6	27.9
22.5 wt% MTMOS	2.76	839	188	32.8	121	27.9
7.5 wt% PTMOS	2.75	210	187	6.84	25.3	27.9
15 wt% PTMOS	2.75	457	187	14.9	55.0	27.9
22.5 wt% PTMOS	2.76	754	188	24.6	90.8	27.9

[a] The HCl reported is volume from a 35 wt% HCl solution.

inorganic and organic solutions, further heat treatments are used to promote additional conversion of the alkoxide xerogel domains via condensation reactions. While Table 1 summarizes the amounts of reactants used in the synthesis of these hybrid materials, the following example is provided for the synthesis of a 22 wt% TMOS hybrid material.

Synthesis of a 22 wt% TMOS hybrid material began by creating a functionalized polyimide solution and a partially hydrolyzed TMOS solution. The functionalized 6FDA–6FpDA–DABA-25 polyimide was created by adding 2.76 g of polyimide to a 150 ml round bottom flask and dissolving it into 27.8 ml of THF. Once the polyimide has completely dissolved, the polyimide was functionalized using 4.35 times the stoichiometric amount of APTEOS (187 μl). This value was based on the total number of polyimide dianhydride endgroups, DABA acid groups, and the minimum amount of APTEOS necessary for gel onset based on a series of cross-linking experiments. The functionalized polyimide solution was then stirred for 30 min at room temperature before mixing with the partially hydrolyzed alkoxide. A separate ^{1}H NMR experiment revealed that at ambient conditions, the reaction between the acid groups in the polyimide and the amine within the APTEOS was complete within 15 min.

The partially hydrolyzed TMOS was generated using a 1:2.6:2.0:0.10 molar ratio of alkoxide, THF, water and acid such that a clear sol–gel is formed within approximately 15 h at ambient conditions. The stoichiometry of the alkoxide, water, and acid was based on half the number of hydrolyzable substituents in the alkoxide. Thus, for MTMOS and PTMOS the molar ratio was 1:2.6:1.5:0.075, but was equivalent to the TMOS molar ratio based on the moles of hydrolyzable substituents. In order to control the exothermic hydrolysis reaction and prevent alkoxide precipitation, a separate solution of water (157 μl), 37.5 wt% HCl (42.5 μl), and THF (1100 μl) was mixed in a 5 ml test-tube. This solution was then slowly added and mixed into a 5 ml test-tube containing 774 μl of TMOS alkoxide, which was then mixed for 30 min before adding it to the functionalized polyimide solution. During the slow addition of this solution to the TMOS, a very noticeable exothermic hydrolysis reaction was observed by an increase in solution temperature. This temperature increase was observed to the largest for MTMOS, followed by TMOS, and finally PTMOS. A THF based solvent system was chosen to compatiblize the alkoxide, water, and HCl and prevent polyimide precipitation. The THF also eliminated unwanted sol precipitation by slowing the condensation reactions that are shown in Fig. 1. Higher alkoxide loading was also possible because alcohol was not used to compatiblize the alkoxide, water, and acid solution, which induce the polymer to precipitate out of the solution. In addition to these benefits, it was assumed that the degree of alkoxide hydrolysis would be enhanced. This is because alcohol is a product during this reaction, and not using it as a solvent medium causes the reaction equilibrium to shift more in favor of hydrolysis instead of esterification.

After the required times were met for the solutions of partially hydrolyzed TMOS sol and functionalized polyimide, the two solutions were then added together and stirred for 1 h at ambient conditions. The resulting homogeneous solution was then filtered with a 5 μm nylon filter, and then solvent cast into a Teflon™ coated pan. The solution was allowed to slowly evaporate for four days (~0.4 ml h^{-1}) at ambient conditions. This extended time interval was chosen to provide sufficient reaction time for the alkoxide sol, and to minimize solvent concentration gradients in the film surface during evaporation. All films underwent a final curing step at vacuum conditions employing heating intervals of 50 °C for 5 h, 150 °C for 5 h, and then 220 °C for 12 h. In general, films had an average thickness of 3 mil or 76.2 μm.

2.4. Material characterization

Thermal stability of the polyimide hybrid materials was assessed using a High-Resolution TA 2950 TGA instrument. Experimental runs were completed on thin films having an average mass of 15 mg. Test conditions included a 20 °C min^{-1} scan rate from 30 to 900 °C with a 20 ml min^{-1} nitrogen purge.

A Rheometric Scientific Mark IV, Dynamic Mechanical Thermal Analyzer, DMTA was used to characterize the glass transition, T_g, and molecular transitions of the polyimides and hybrid materials. Experimental runs were completed on film samples having dimensions of $15 \times 4 \times 0.07\ mm^3$. The run conditions were conducted at a strain of 0.01%, a constant static force of 0.015 N, and a heating rate of 2 °C min^{-1} in air. The low strain and force were chosen in order to ensure a linear viscoelastic response during an experimental run, and the sample dimensions were set to exceed a length to width ratio of three to minimize sample edge effects during the DMTA test.

Nuclear magnetic resonance spectrometer, Varian Unity 400, was employed to collect ^{13}C spectra. The NMR was primarily used to confirm the molecular structure of polyimides synthesized, to evaluate the DABA content, and to determine quantitatively the percent imidization. All samples were dissolved to a concentration of approximately 60 mg of polymer per ml of hydrogenous NMP.

Fourier transform infrared spectroscopy (FTIR) was employed to confirm the conversion of polyamic acid to polyimide and to assess the overall chemical changes in the hybrid organic–inorganic material after the sol–gel process. A BIO-RAD FTS-40A FTIR spectrometer, equipped with high sensitivity liquid nitrogen cooled MCT detector was employed for this purpose. Attenuated total reflectance FTIR (ATR-FTIR) spectra of thin polyimide films were collected with 4 cm^{-1} resolution. The angle of incidence was 45° and the crystal employed was a KRS-5 SPP.

Molecular weights and molecular weight distribution of the polyimide were evaluated with a Waters 150C GPC/ALC chromatograph. This instrument was equipped with HT2 + HT3 + HT4 Waters Styragel columns and a differential refractometer and viscometer detector. Samples were prepared using 4 mg of polymer per milliliter of NMP solution containing 0.02 M P_2O_5. A 200 μl sample was injected into the instrument that operated at a constant temperature of 60 °C and used NMP as the eluting solvent at a flow-rate of 1.0 ml min^{-1}. A universal calibration curve was generated from narrow molecular weight polystyrene standards purchased from Polymer Laboratories Inc.

Water absorption experiments were performed on thin polyimide and hybrid material films that were dried for seven days at 180 °C in a vacuum oven prior to contact with water. These rectangular samples had nominal length of 35 mm, a width of 25 mm, and a thickness of 0.06 mm with masses ranging from 100 to 180 mg. This sample geometry was chosen in order to have a relatively high surface area to volume ratio (128) to assist in the attainment of water absorption equilibrium. Absorption experiments were performed at 25 °C and were considered complete after 10 days of immersion in deionized water. At the end of the experiment, the samples were quickly removed from the water, blotted dry, and immediately weighed to determine the total water uptake.

Density measurements were based on Archimede's principle and the data were collected utilizing a Mettler AJ100 analytical balance fitted with a Mettler ME-33360 density determination kit. Samples for density measurements were thin films having masses ranging from 80 to 160 mg that were dried for 24 h at 180 °C in a vacuum oven prior to measurements. Isooctane was the liquid medium for all these samples.

Transmission electron microscope, a Philips 420T TEM operating at 100 kV and an atomic force microscope was employed in evaluating the hybrid morphology.

3. Results

3.1. Results of FTIR and NMR studies

The reaction conditions utilized to convert the polyamic acid to the polyimide were semi-qualitatively assessed as a function of conversion and time based on a 66K $\bar{M}_w$ 6FDA–6FpDA polyimide. The FTIR spectra of the conversion of this 6FDA–6FpDA polyamic acid to polyimide are shown in Fig. 5. Fig. 5 clearly shows how the polyamic acid peak at 1690 cm^{-1} disappears as the 6FDA–6FpDA was converted to a polyimide based on the solution imidization technique. However, since FTIR is not sensitive enough to detect low concentrations of polyamic acid in the polyimide structure, the reaction was carried out for 24 h. Because the 6FDA–6FpDA–DABA-25 polyimide was primarily composed of 6FDA–6FpDA units, the conversion study of the 6FDA–6FpDA was considered directly applicable to the conversion time necessary for the 6FDA–6FpDA–DABA-25 polyimide. Fig. 8 also can be used to semi-qualitatively demonstrate that the 6FDA–6FpDA–DABA-25 polyimide is completely imidized based on the absence of the polyamic acid absorption peak at 1690 cm^{-1}. In order to complete the

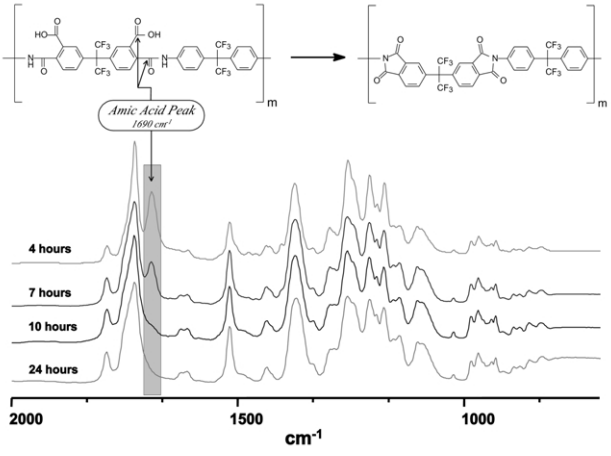

Fig. 5. FTIR spectra of the conversion of a polyamic acid to a polyimide at 180 °C as a function of time for 66 $\bar{M}_w$ 6FDA–6FpDA polyimide. Polyimides were solution cast from CH_2Cl_2 onto KBr crystals.

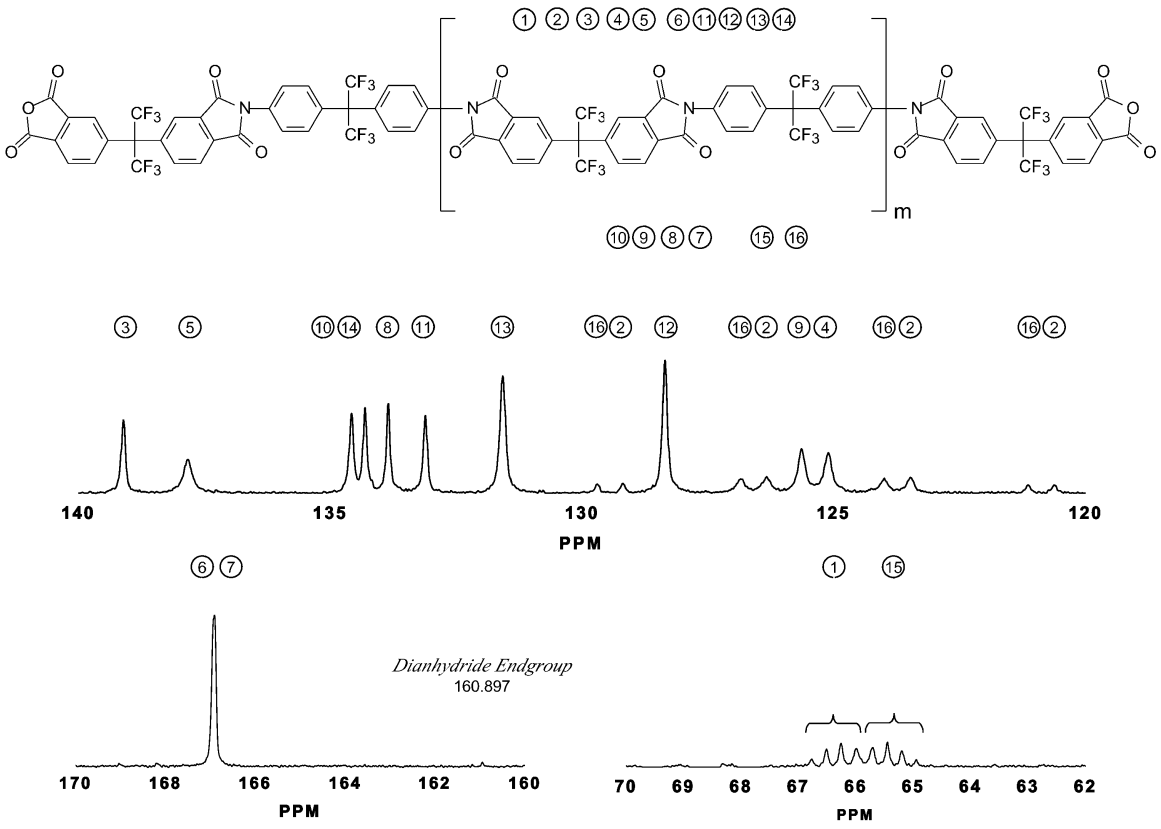

Fig. 6. Solution ^{13}C NMR of 6FDA–6FpDA polyimide in hydrogenous NMP.

characterization of the 6FDA–6FpDA–DABA-25 polyimide, solution ^{13}C NMR was completed on this polyimide and a 66K $\bar{M}_w$ 6FDA–6FpDA polyimide to verify carbon chemical shifts. Fig. 6 shows the chemical shifts of the 6FDA–6FpDA polyimide, which proved to be essential for the assignment of chemical shifts due the DABA moiety. Fig. 7 is the final ^{13}C NMR spectrum of the 6FDA–6FpDA–DABA-25 polyimide, which completely identifies the structure of the polyimide, and within the sensitivity of this technique, indicates a completely imidized structure. Figs. 6 and 7 also shows the chemical shift of 160.90 ppm associated with an unreacted dianhydride group, which also provides evidence that 6FDA–6FpDA–DABA-25 polyimide has 6FDA dianhydride endgroups. Finally, integration of the spectra in Fig. 7 also semi-qualitatively revealed that the polyimide contained 25.1 mol% DABA. While not shown, the chemical shift due to incomplete imidization typically observed near 172 ppm was absent from the 6FDA–6FpDA–DABA-25 polyimide. Based upon the results from FTIR and ^{13}C NMR, the 6FDA–6FpDA–DABA-25 polyimide is believed to be fully imidized, and successfully synthesized in this study.

The FTIR absorbance spectra of hybrid materials based on 80K $\bar{M}_w$ 6FDA–6FpDA–DABA-25 polyimide and TMOS, MTMOS and PTMOS alkoxides are shown in Figs. 8–10. These spectra were used to evaluate modifications in the local environment of the polyimide caused by interfacial interactions with the inorganic domains, and to differentiate between the different types of alkoxides employed in this study. FTIR was also used to verify imidization of the polyamic acid by observing the disappearance of the amide carbonyl at 1690 cm^{-1} and the growth of the imide carbonyl band at 1720 cm^{-1}. Complete imidization was also confirmed with ^{13}C NMR.

Silica xerogel to glass conversion occurs near 700 °C, a temperature far above the 220 °C employed in the curing of the alkoxide systems [22]. The variations in the silicate chemistry can be quantitatively inferred from the ATR spectra [33–35]. For example, spectra of hybrid materials based on TMOS, shown in Fig. 8, shows the presence of the Si–O–Si stretching band, ranging from 1000 to 1100 cm^{-1}, which is associated with open chain structures, as well as a silanol stretching band, Si–OH, which occurs from 1020 to 1040 cm^{-1}. Absorption stretches associated with Si–O–Si cyclic structures present in the 1080–1090 cm^{-1} region are also observed in this hybrid material [33]. Although these bands overlap, relative comparison of the various spectra suggest that the main type of structures present in the TMOS derived silica are condensed species, followed by silanol groups and to a smaller extent open chain structures. These conclusions are consistent with previous studies, which argue that acid catalysis favors hydrolysis and point

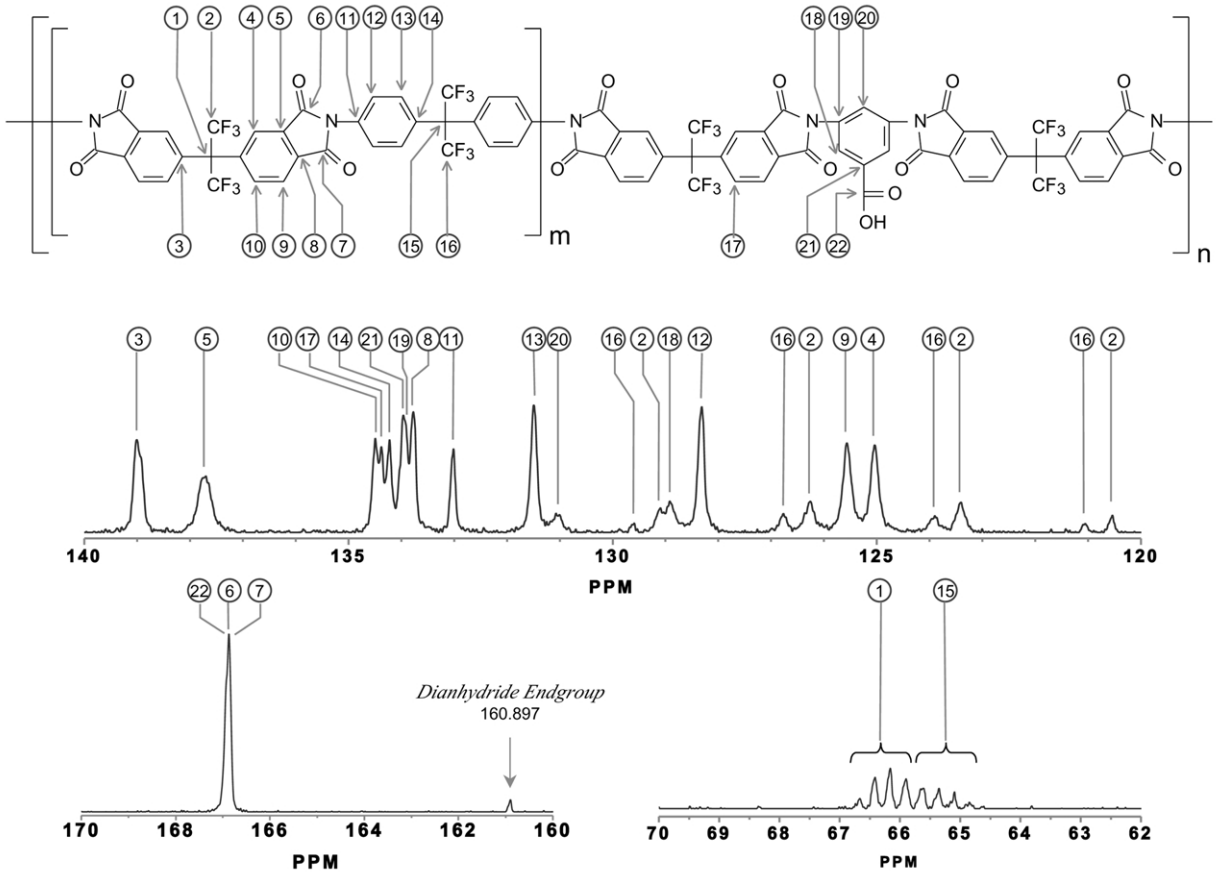

Fig. 7. Solution ^{13}C NMR of 80K $\bar{M}_w$ 6FDA–DABA-25 in hydrogenous NMP.

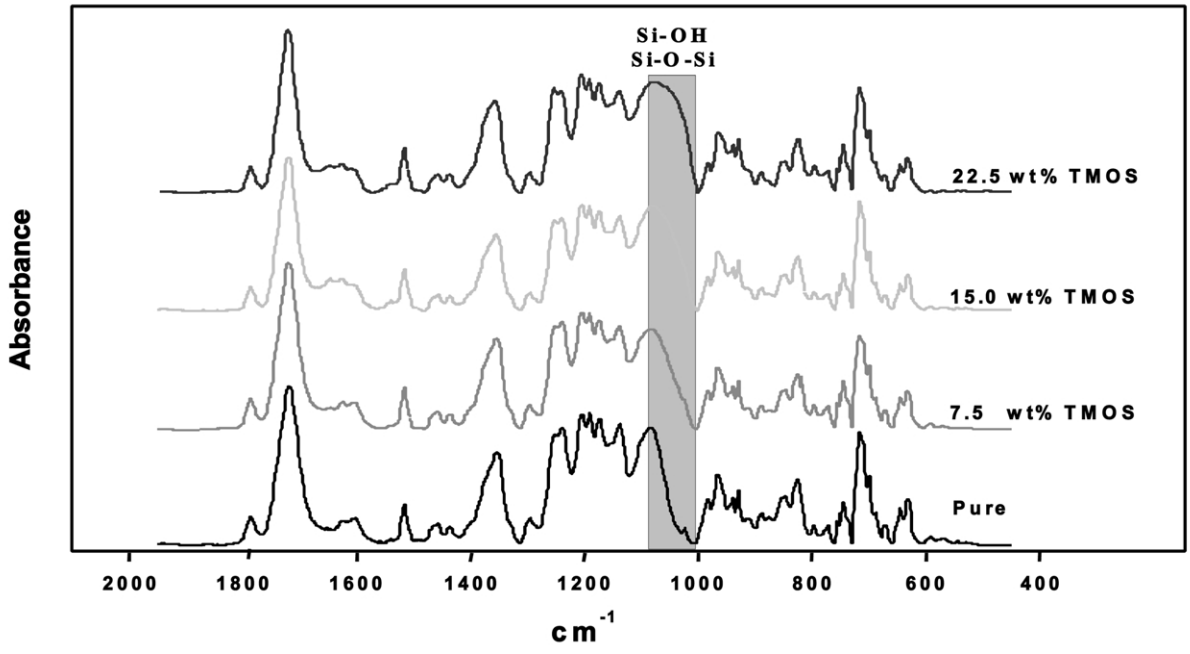

Fig. 8. ATR-FTIR spectrum of hybrid material based on a 80K $\bar{M}_w$ 6FDA–DABA-25 polyimide and TMOS showing Si–OH and Si–O–Si stretching associated with TMOS derived silica.

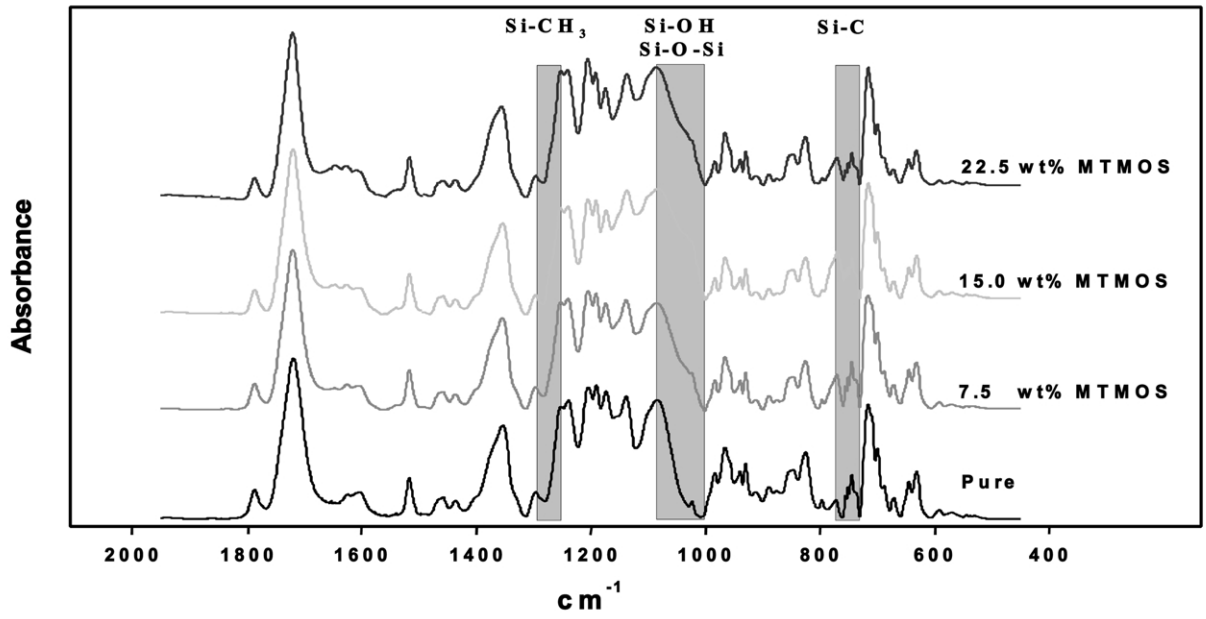

Fig. 9. ATR-FTIR spectrum of hybrid material based on a 80K $\bar{M}_w$ 6FDA–DABA-25 polyimide and MTMOS showing Si–OH, Si–O–Si, Si–C, and Si–CH_3 silica domain stretching.

out that as the solvent concentration decreases condensation is enhanced [21,25]. Therefore, we conclude that the final TMOS silica material was a hydrolyzed and tightly cross-linked structure. This conclusion is consistent with the measured pure bulk density of the TMOS, which was 1.80 g ml^{-1}. A separate study completed by Spinu indicated that in the case of TMOS-polyimide hybrid materials, the presence of the organic species can actually catalyze the silica condensation reaction [28]. Although these results are dependent on the alkoxide and reaction conditions, we expect that some catalytic behavior could have also contributed in this case.

In contrast to TMOS-based hybrid materials, the silica structures present in MTMOS-derived hybrid systems must be quite different as evidenced from the ATR spectra, shown in Fig. 9. Again, we see the Si–O–Si stretching ranging from 1000 to 1100 cm^{-1} associated with open chain structures, although the relative intensity of this

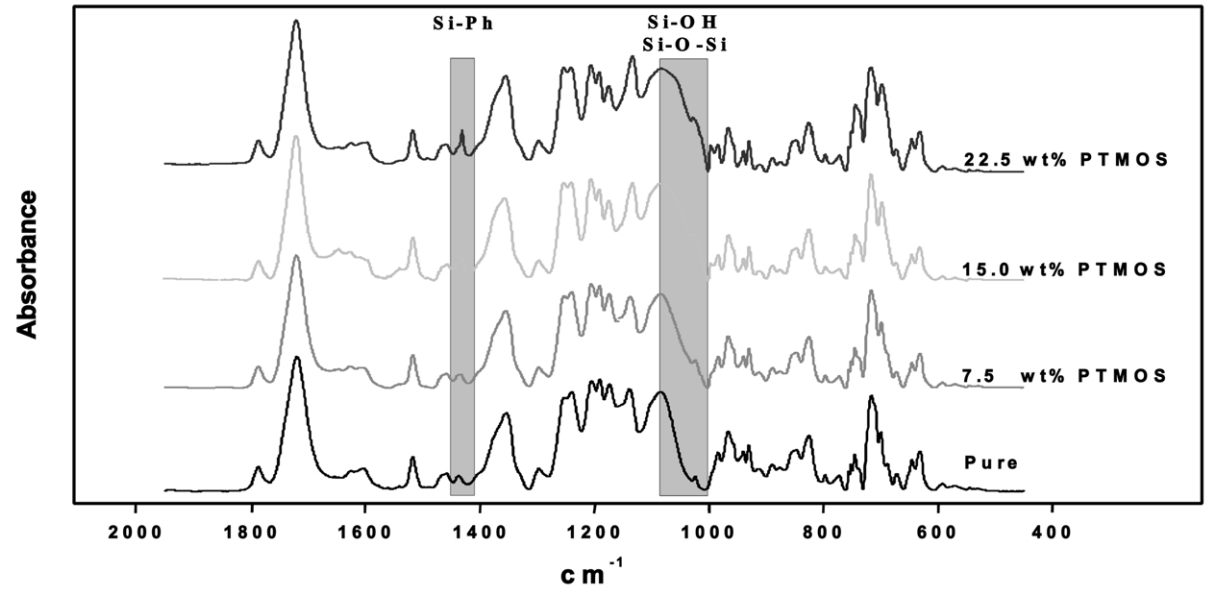

Fig. 10. ATR-FTIR spectrum of hybrid material based on a 80K $\bar{M}_w$ 6FDA–DABA-25 polyimide and PTMOS showing Si–OH, Si–O–Si, Si–C, and Si–Ph silica domain stretching.

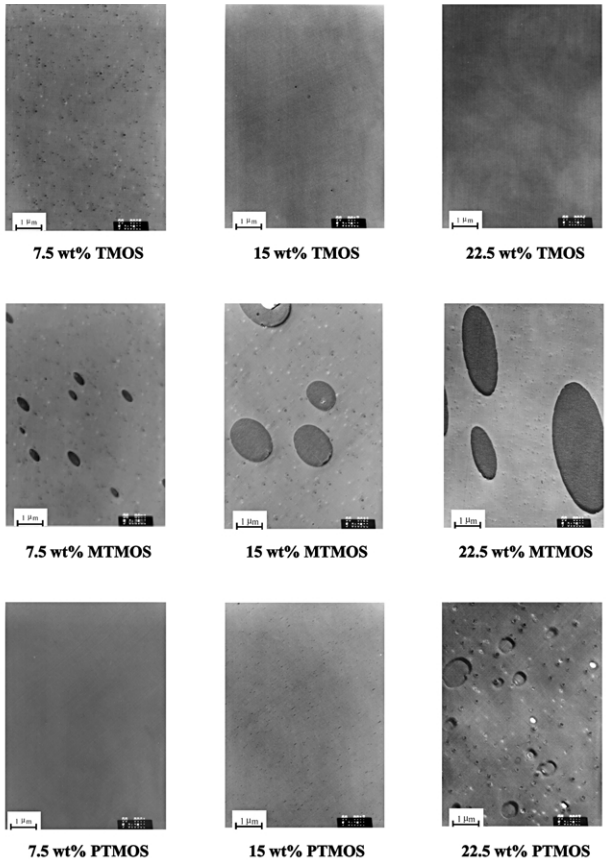

Fig. 11. TEM images of hybrid systems based on 80K $\bar{M}_w$ 6FDA–DABA-25 polyimide. TEM images are cross-sections of films at a magnification of 18 500×.

band is much lower than in the TMOS derived systems. The open chain structures in the MTMOS derived silica arise because of the lower functionality ($f = 3$), and the steric hindrance introduced by the methyl group. The silanol group absorptions ranging from 1020 to 1040 cm^{-1} is indicative of uncondensed Si–OH groups. Thus, we conclude that the silica generated by MTMOS was somewhat hydrolyzed and loosely cross-linked. The measured pure bulk density of MTMOS was 1.20 g ml^{-1}, which is significantly lower than the density observed in the TMOS systems.

Finally, the ATR-FTIR spectra of PTMOS based silica structures formed in these hybrid systems are shown in Fig. 10. The contributions of the Si–OH and Si–O–Si vibrational bands associated with open chain structures are lower in intensity when compared to the other alkoxide systems, suggesting even lower degree of hydrolysis and condensation. These features are produced by the PTMOS functionality of $f = 3$ and significant steric hindrances introduced by the large phenyl group. An 'inductive effect' introduced by the phenyl group could have also contributed to the lower hydrolysis in the PTMOS system. In addition, the observation of a Si–O–C absorption at 997 cm^{-1} indicates the presence of unhydrolyzed methoxy substituents, supporting the idea of incomplete hydrolysis. Hence, the PTMOS derived silica was incompletely hydrolyzed and poorly condensed, which was also consistent with the measured low pure PTMOS bulk density of 1.28 g ml^{-1}.

Unfortunately, because the silicon absorptions overlap with each other and substantially with the polyimide absorptions, we were able to only qualitatively accentuate the main structural differences associated with TMOS, MTMOS and PTMOS silica systems.

3.2. TEM results

Results of transmission electron microscopy studies of the hybrid materials are shown in Fig. 11. Interestingly, of the three different types of systems, the MTMOS-based hybrids show the largest degree of phase separation. The

Table 2
80K $\bar{M}_w$ 6FDA–6FpDA–DABA-25 polyimide and hybrid material property summary

	TGA[a] (°C)	Residue[a] (%)	ρ[b] (g ml^{-1})	H_2O uptake[c] (g_{Water}/g_{Hybrid})	NMP uptake[d] (g_{NMP}/g_{Hybrid})
6FDA–6FpDA–DABA-25	430	49.3	1.486	2.01	5.72[e]
7.5 wt% TMOS	435	46.2	1.500	1.57	[f]
15 wt% TMOS	379	42.9	1.505	2.13	2.47
22.5 wt% TMOS	408	42.4	1.522	3.13	0.22
7.5 wt% MTMOS	463	47.4	1.476	0.69	12.5
15 wt% MTMOS	449	44.5	1.460	0.89	[f]
22.5 wt% MTMOS	422	41.7	1.442	1.94	1.92
7.5 wt% PTMOS	440	46.3	1.471	0.90	10.5
15 wt% PTMOS	410	41.3	1.458	1.34	2.45
22.5 wt% PTMOS	452	40.1	1.433	0.99	[f]

[a] TGA, temperature corresponding to 5% weight loss, value has ~10% error.
[b] Density, data collected at 25 °C, ~0.12% error.
[c] Water absorption data, ~10% error.
[d] Swelling data, ~10% error.
[e] Data collected from a pure crosslinked sample.
[f] Sample swelled to such a degree that measurement was not possible based on sample size.

MTMOS silica structures appear as micron-sized dark ovals, which increase in size with increasing MTMOS content. In addition, smaller silica domains in the order of several hundred nanometers are dispersed throughout the polyimide matrix. The morphology of the hybrids based on the TMOS alkoxide, on the other hand, is quite homogeneous, appearing as a very fine dispersion of silica particles at the lowest TMOS concentration and as a fine interpenetrating phase at 22.5 wt% TMOS. Because TMOS has the highest reactivity of the three systems [21,22], it quickly undergoes hydrolysis and cross-links in solution before phase separation can take place. This gives rise to a highly interpenetrating network of polymer and silica structures. The loosely cross-linked MTMOS silica structures are much slower to form, allowing the small MTMOS molecules to phase separate before the sol–gel reactions are complete. It is possible, that some polymer chains also become trapped in the silica structures, as suggested by the results of mechanical studies to be discussed later. The PTMOS-based hybrid systems are the slowest to react [21,22] and the slowest to diffuse, although some phase separation is evident in the 22.5 wt% PTMOS hybrid system as well. Silica domains that did form in the PTMOS-based systems, as a result of the hydrolysis and condensation reactions, appear as sub-micron-sized particles with low contrast due to the presence of the phenyl groups. However, as pointed out in the discussion of the FTIR results, it is highly probable that most PTMOS molecules remain dispersed throughout the hybrid system as unhydrolyzed and uncross-linked moieties.

3.3. Hybrid inorganic–organic physical properties

In order to evaluate the effect of the various silica structures within the pure polyimide, the thermal stability, density, water absorption, and solvent swelling characteristics were determined. The oxidative stability of these hybrid materials is summarized in Table 2. While all these hybrid materials reveal excellent thermal stability at elevated temperatures, at 5% weight loss, the temperatures are effectively the same within the experimental error of the measurement. However, the percent of carbonaceous residue at 900 °C decreases with increasing inorganic content for all the alkoxides explored in this study. This decrease in carbonaceous residue with increasing inorganic content is attributed to the incomplete silica conversion at processing temperatures, also qualitatively observed with FTIR. Consequently, once the temperature is increased above the curing temperature of the hybrid materials, volatile products from the condensation reactions of the silicon alkoxides are driven off. Furthermore, both MTMOS and PTMOS hybrid systems have lower residues than TMOS because the methyl and phenyl groups also can pyrolyze. The PTMOS system has the lowest residue of the alkoxide series because of the larger mass of the phenyl leaving unit.

The density of the TMOS based hybrid materials increased with increasing content, while the density of both MTMOS and PTMOS hybrid materials decreased with increasing content. These results are directly attributed to the additive contribution of the density of the inorganic materials, which were 1.80 g ml^{-1} for TMOS, 1.20 g ml^{-1} for MTMOS, and 1.28 g ml^{-1} for PTMOS. Statistical analysis of the density data by a simple 'rule of mixtures' suggested that the density of the polyimide does not change in the presence of the silica structures.

Water absorption studies were carried out on these hybrid materials to probe the extent of hydrolysis and condensation reactions. In addition to this, the effects of the aliphatic and aromatic methyl and phenyl groups in MTMOS and PTMOS on the hydrophilicity of the materials were

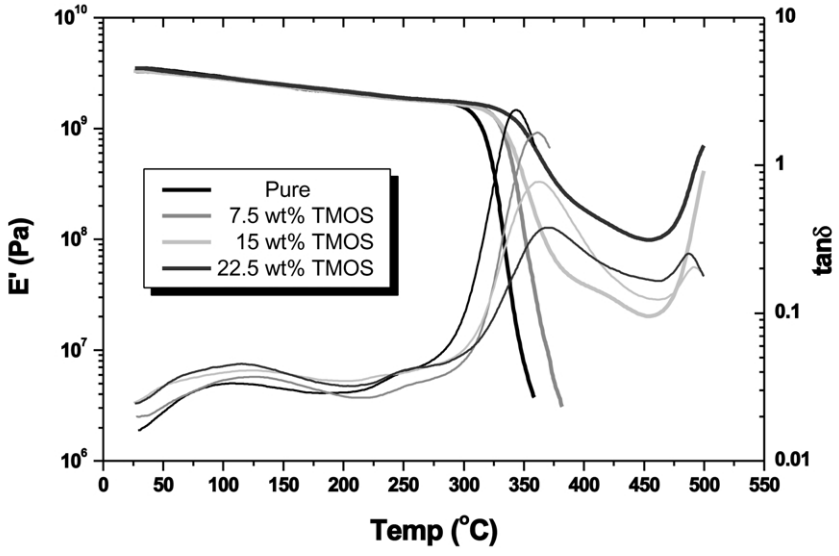

Fig. 12. E' and tan δ for a 80K $\bar{M}_w$ 6FDA–DABA-25 polyimide and hybrid materials containing 7.5, 15, and 22.5 wt% TMOS. Data was collected from the first scan at 2 °C min^{-1}, 0.01% strain, and a constant static force of 0.015 N with an air purge.

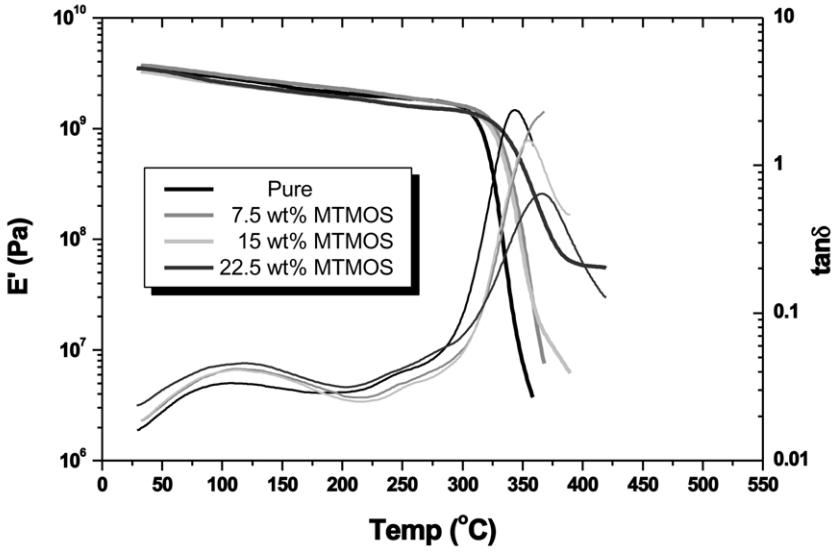

Fig. 13. E' and tan δ for a pure 80K $\bar{M}_w$ 6FDA–DABA-25 polyimide and hybrid materials containing 7.5, 15, and 22.5 wt% MTMOS. Data was collected from the first scan at 2 °C min^{-1}, 0.01% strain, and a constant static force of 0.015 N with an air purge.

examined with this experiment. The results of the water absorption experiments are listed in Table 2. Clearly, the presence of the aliphatic and aromatic character of the inorganic domains reduced the water uptake by as much as 290% for MTMOS and 220% for PTMOS. However, the TMOS based hybrid materials had an increase in water uptake as high as 160%, which was attributed to the high concentration of silanol groups. This result clearly demonstrates the competing effects of the silanol groups and the aliphatic and aromatic character of the alkyl groups in the inhibition or enhancement of water absorption. Indeed, the differences in water absorbency among these alkoxides could be utilized to control the hydrophobic or hydrophilic properties of these hybrid materials.

Table 3
Data summary of an 80K $\bar{M}_w$ 6FDA–DABA-25 polyimide and corresponding hybrids

	α'	T_g[a] (α)		β[a]		T_g[b]
	°C	°C	tan δ	°C	tan δ	°C
6FDA–6FpDA–DABA-25	–	344	2.365	110	0.0335	303
7.5 wt% TMOS	–	362	1.654	126	0.0372	326
15 wt% TMOS	491	363	0.777	123	0.0410	322
22.5 wt% TMOS	488	370	0.378	113	0.0455	340
7.5 wt% MTMOS	–	364	2.147	117	0.0419	330
15 wt% MTMOS	–	355	1.474	113	0.0412	326
22.5 wt% MTMOS	–	366	0.634	118	0.0457	340
7.5 wt% PTMOS	–	359	1.716	122	0.0439	321
15 wt% PTMOS	–	370	0.678	127	0.0429	337
22.5 wt% PTMOS	491	359	1.167	120	0.0415	328

[a] DMTA, data collected at 2 ° min^{-1} in air and 0.01% strain. Error ~ 0.2%.

[b] DSC, data collected at 10 ° min^{-1} in air and second heating ramp. Error ~ 0.7%.

In order to assess the degree of inorganic interpenetration into the polyimide matrix, swelling experiments in NMP were also performed on thin cross-linked polyimide and hybrid films. These experiments suggest that significant reductions in the swelling of material are possible and depend on the type of alkoxide employed in the synthesis of the hybrid material. While a cross-linked polyimide sample swelled 572%, TMOS based hybrids were capable of minimizing the swelling down to 22%. The solvent swelling behavior of MTMOS and PTMOS hybrid materials were mixed with minimum swelling occurring at 22.5 wt% MTMOS and 15 wt% PTMOS, and significant swelling at 15 wt% MTMOS and 22.5 wt% PTMOS, which prevented measurements. The differences in solvent swelling among these hybrid materials are attributed to the degree of interpenetration of the silica structures into the polyimide matrix and the degree of covalent bonds formed with the polyimide matrix. These differences are a consequence of the degree of hydrolysis, functionality, and morphology of the inorganic domains formed from the various alkoxides surveyed. Because TMOS has the highest functionality ($f = 4$) and reactivity of all the alkoxides studied, it was expected that the silica domains would have the highest probability of interpenetrating and forming a higher cross-link density within the polyimide matrix. This may be a reasonable explanation for the observed swelling reduction in the TMOS based hybrids. Likewise, the lower functionality ($f = 3$) and slower reaction kinetics of MTMOS and PTMOS precluded them from forming the higher cross-link density required for significant swelling reduction. Overall, the swelling behavior is believed to be a function of the cross-link density and solubility of the polymer and alkoxide. Together, these traits could be used to create materials that have significant improvements in solvent resistance.

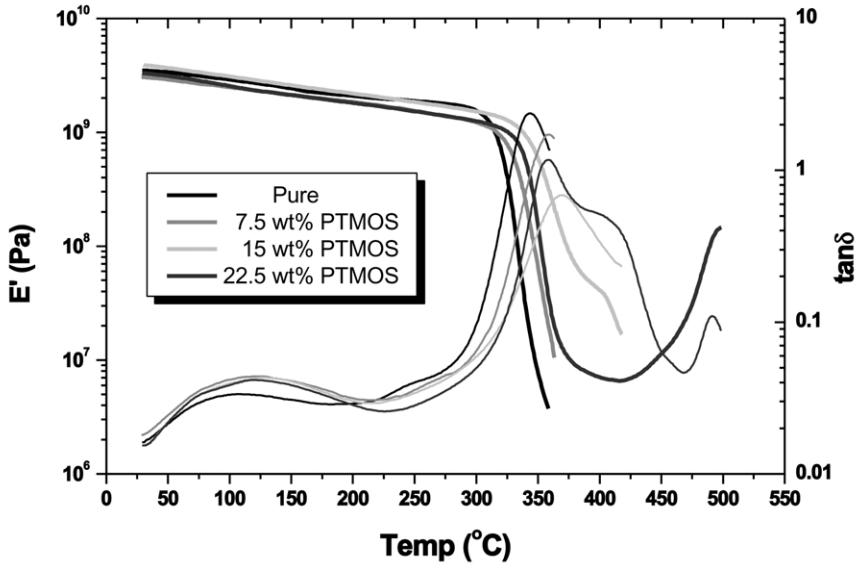

Fig. 14. E' and tan δ for a pure 80K $\bar{M}_w$ 6FDA–DABA-25 polyimide and hybrid materials containing 7.5, 15, and 22.5 wt% PTMOS. Data was collected from the first scan at 2 °C min^{-1}, 0.01% strain, and a constant static force of 0.015 N with an air purge.

3.4. Hybrid mechanical properties

Figs. 12–14 shows the storage modulus, E', as a function of temperature for the various hybrid materials. Both TMOS and PTMOS hybrid systems at higher inorganic concentrations revealed significant changes in E' as a function of temperature above their T_g. The region above the T_g is known as the rubbery plateau, which is proportional to the molecular weight of the polymer. The rubbery plateau for TMOS at 15 and 22.5 wt%, and PTMOS at 22.5 wt% is not constant, but rises dramatically with increasing temperature near 460 °C for TMOS and 410 °C for PTMOS based hybrids. Since the magnitude of E' in this region is related to the molecular weight, it is believed that additional cross-linking occurs at these elevated temperatures due to further inorganic condensation reactions and covalent bonding with the polyimide. Some polymer degradation also occurs above 400 °C. MTMOS based hybrid materials did not demonstrate the plateau behavior in E' at any composition. This may be primarily due to the highly phase separated inorganic domains observed in the TEM morphology, which would decrease the degree of interpenetration into the polyimide matrix. Of all the hybrid materials observed in this study, only MTMOS based hybrid materials had the greatest degree of phase separation of the alkoxide series.

The alkoxide type and content also have an effect on the cooperative motions of the polymer chains at T_g. These results are summarized in Table 3, and Figs. 12–14. In general, the T_g of the hybrid materials increased with increasing inorganic content by 11–26°C, however no clear trend with alkoxide concentration was observed. Typically, the T_g of a simple particle filled system rises with increasing particle content. The fact that this trend was not observed here may reflect the variability in the degree of cross-linking and morphology of these systems.

The magnitude of tan δ at T_g is a measure of the energy-damping characteristic of a material, and the breadth of the tan δ relaxation is indicative of the cooperative nature of the relaxation process of the polymer chains [34–36]. Conceptually, cooperativity can be related to the ease at which polymer chains move in concert through the glass transition, while non-cooperative materials have polymer chains that resist concerted motion that are characterized by very broad tan δ [34–36]. The magnitude of tan δ decreased with increasing inorganic content for all the hybrid materials, and the greatest tan δ decreases were associated with the TMOS based hybrids, followed by MTMOS and PTMOS based hybrids. In general, decreasing magnitude of tan δ with increasing particle concentration is a typical behavior for a particle filled system. However, the breadth of tan δ through the T_g of these materials is characterized by small to very significant broadening and additional transitions above the T_g were observed for TMOS and PTMOS based hybrids. While MTMOS based hybrid materials had an increasing tan δ breadth with increasing inorganic content, TMOS based hybrid materials had significant broadening of the breadth of tan δ and a new α' transition at 491 and 488 °C for 15 and 22.5 wt% TMOS. At low PTMOS contents the breadth of tan δ increased with increasing content. However, at 22.5 wt% PTMOS there is not only broadening of tan δ, and a new α' transition at 491 °C, but a significant tan δ shoulder at 400 °C is observed, which is indicative of another molecular transition. Separate relaxations are

typically observed in partially miscible polymer blends, where the individual T_gs tend to merge into one as the compatibility of the blend increases [36–38]. The tan δ shoulder at 400 °C suggests the presence of an inorganic–organic phase, which may have a higher T_g than the polyimide. The presence of the α' transitions in the TMOS and PTMOS hybrid materials may also be a consequence of additional inorganic condensation and cross-linking reactions with the polyimide matrix, which are taking place at higher DMTA testing temperatures. Tsaganopolulos et al. have observed two tan *delta* peaks in several polymers filled with very fine silica particles. One was related to the usual polymer glass transition, while the peak occurring at higher temperature was assigned to the glass transition of regions containing chains of reduced mobility [39].

The beta relaxation, β, occurs below the T_g and is associated with local bond rotations and molecular segment motions along the polymer backbone, and the magnitude of this relaxation is proportional to the concentration of segments contributing to the relaxation [38]. In general, these motions are considered to be primarily a function of the type of diamine in the polyimide, and their presence and magnitude have been ascribed to several material properties [36–38]. In our experiments, two observations were made regarding the incorporation of inorganic domains into these hybrid materials. The first was that the number of polymer segments in motion increased with increasing inorganic content, which is evident from the increase in tan δ at the β relaxation. The second observation was that the temperature of the β transition increased with the addition of inorganic material, which indicates that a higher energy barrier exists for these molecular motions. Overall, the observed changes in the α and β relaxations suggest that the presence of the silica domains retards cooperative motions of the polymer chains and facilitates small-scale motions, possibly because of changes in the molecular packing arrangements. Similar conclusions were reached by Bershtein et al. who have looked at the segmental dynamics and thermal stability of polyimide–silica hybrids prepared by the site isolation method [40]. Bershtein has suggested that most of the polyimide chains were in fact immobilized on the silica surface, decreasing the number of Kuhn segments available for relaxational motions.

DSC was also used to evaluate the changes in T_g as a function of alkoxide type and content of these hybrid materials, which is summarized in Table 3. Although there is an 18–37°C change in T_g with the introduction of different alkoxide types and amounts, there does not appear to be a direct correlation with the nature and content of the alkoxide and the T_g. We believe that the lack of a clear trend is a consequence of competing effects taking place during membrane formation. One effect is the restriction of polymer chain motion due to cross-linking and the other is the incomplete alkoxide condensation, which introduces unreacted methoxy and alkyl groups into the polymer matrix, enhancing polymer chain motion.

4. Conclusions

An alternative synthetic route was developed and evaluated in order to fabricate hybrid materials with high mechanical integrity, which would enable them to be formed into defect-free dense films. The morphology of these hybrid materials was largely dependent on the type of alkoxide precursor employed in the synthesis. For example, TMOS based hybrids were very homogeneous, while the MTMOS and PTMOS based hybrids were phase separated, owing to the different reaction rates and functionalities of the precursors. The silica structures in the MTMOS and PTMOS based hybrid systems were also incompletely condensed, resulting in lower degree of cross-linking with the polyimide matrix, when compared to the TMOS based materials. The TGA results indicated that the thermal stability changed very little with the introduction of the alkoxides. Swelling and water absorption experiments suggested that this synthetic approach might be used to create solvent resistant materials, having controlled hydrophobic character. The results of DMTA studies pointed to the existence of another partially miscible inorganic–organic phase, which had a higher T_g than the polyimide. We are tempted to think that this phase represents the interfacial region between the silica structures and the polyimide matrix. Observed changes in the α and β relaxations suggested that the presence of the silica domains also retarded cooperative motions of the polymer chains, and facilitated small-scale molecular motions. This could be possibly due to changes in the molecular packing arrangements, which were propagated from the silica surface to the bulk of the polyimide matrix.

Acknowledgements

The authors would like to thank the National Science Foundation for support of this project via CTS-9905549. Additional support for C. Cornelius was provided by the Eastman Chemical Fellowship in Polymer Chemistry, the General Electric Academic Fellowship and the Oneida Tribe of Wisconsin. Many thanks are also extended to Dr Steve McCartney for his help with the TEM microscopy.

References

[1] Wung CJ, Yang Y, Prasad PN, Karasz FE. Polymer 1991;32:605–8.
[2] Krug H, Schmidt H. New J Chem 1994;18:1125–34.
[3] Khastgir D, Maiti HS, Bandyopadhyay PC. Mater Sci Engng 1988;100:245–53.
[4] Philipp G, Schmidt H. J Non-cryst Solids 1984;63:283–92.
[5] Wang S, Mark JE. Polym Bull 1992;29:343–8.
[6] Wang B, Wilkes GL. J Macromol Sci, Pure Appl Chem 1994;A31:249–60.
[7] Nagasaki Y, Hashimoto Y, Kato M, Kimijima T. J Membr Sci 1996;110:91–97.
[8] Smaihi M, Jermoumi T, Marignan J, Noble RD. J Membr Sci 1996;116:211–20.

[9] Guizard C, Heckenbenner P, Schrotter JC, Hovnanian N, Smaihi M. Better ceramics through chemistry VII: organic/inorganic hybrid materials. Mater Res Soc Symp Proc 1996;435:283–94.
[10] Schrotter JC, Smaihi M, Guizard C. J Appl Polym Sci 1996;61(2):2137–49.
[11] Joly C, Goizet S, Schrotter JC, Sanchez J, Escoubes M. J Membr Sci 1997;130:63–74.
[12] Huang HH, Orler B, Wilkes GL. Macromolecules 1987;20:1322–30.
[13] Wang B, Wilkes GL. J Polym Sci, Part A: Polym Chem 1991;29:905–9.
[14] Brinker CJ, Scherer GW. Sol–gel science; the physics, chemistry of sol–gel processing. San Diego: Academic Press, 1990.
[15] Saegusa T. Pure Appl Chem 1995;12:1965–70.
[16] Chujo Y, Ihara E, Kure S, Saegusa T. Macromolecules 1993;26(21):5681–6.
[17] Fitzgerald JJ, Landry CJ, Pochan JM. Macromolecules 1992;25:3715–22.
[18] Landry CJT, Coltrain BK, Wesson JA, Zumbulyadis N, Lippert JL. Polymer 1992;33:1496–506.
[19] Landry CJT, Coltrain BK, Brady BK. Polymer 1992;33:1486–95.
[20] Mark JE, Jiang CY, Tang MY. Macromolecules 1984;17:2613–6.
[21] Sanchez C, Ribot F. New J Chem 1994;18:1007–47.
[22] Livage J, Henry M, Sanchez C. Prog Solid State Chem 1988;18:250–341.
[23] James PF. J Non-Cryst Solids 1988;100:93–114.
[24] Ying Y, Benziger J. J Am Ceram Soc 1993;76:2571–82.
[25] Iler RK. The chemistry of silica. New York: Wiley, 1979.
[26] Mascia L. Trends Polym Sci 1995;3:61–70.
[27] Morikawa A, Iyoku Y, Kakimoto M, Imal Y. Polym J 1992;24:107–13.
[28] Spinu M. Silicon-based organic and inorganic polymers. PhD Thesis, Virginia Polytechnic Institute and State University, 1991.
[29] Nandi M, Conklin JA, Salvati Jr L, Sen A. Chem Mater 1991;3:201–6.
[30] Morikawa A, Iyoku Y, Kakimoto M, Imal Y. J Mater Chem 1992;2:679–90.
[31] Kioul A, Mascia L. J Non-Cryst Solids 1994;175:169–86.
[32] Ghosh MK, Mittal KL. Polyimides: fundamentals and applications. New York: Marcel Dekker, 1996.
[33] Alpert NL, Keiser WE, Szymanski HA. IR theory and practice of infrared spectroscopy. New York: Plenum Press, 1973.
[34] Mauritz KA, Warren M. Macromolecules 1989;22:1730–4.
[35] Matos MC, Ilharco LM, Almeida RM. J Non-Cryst Solids 1992;147, 148:232–7.
[36] Cowie JMG. Polymers: chemistry and physics of modern materials. 2nd ed. New York: Blackie/Chapman & Hall, 1994.
[37] Matsuoka S. Relaxations in polymers. New York: Oxford University Press, 1992.
[38] Aklonis JJ, MacKnight WJ. Introduction to polymer viscoelasticity. 2nd ed. New York: Wiley, 1983.
[39] Tsagaropolulos G, Eisenberg A. Macromolecules 1995;28:6067–77.
[40] Bershtein VA, Egorova LM, Sysel P, Yakushev PN. Polym Sci, Ser A 2000;42:788–94 (translated from Vysokomolekularnye Soedineniya, Ser A 2000;42(7):1192–9).